Letter

Interaction-enhanced topological Hall effects in strained twisted bilayer graphene

Pierre A. Pantaleón,[1,*] Võ Tiến Phong,[2,†] Gerardo G. Naumis,[3] and Francisco Guinea[1,4,5]

[1]*IMDEA Nanoscience, Faraday 9, 28049 Madrid, Spain*

[2]*Department of Physics and Astronomy, University of Pennsylvania, Philadelphia, Pennsylvania 19104, USA*

[3]*Departamento de Sistemas Complejos, Instituto de Física, Universidad Nacional Autónoma de México, Apdo. Postal 20-364, 01000, Ciudad de México, CDMX, México*

[4]*Donostia International Physics Center, Paseo Manuel de Lardizábal 4, 20018 San Sebastián, Spain*

[5]*Ikerbasque, Basque Foundation for Science, 48009 Bilbao, Spain*

(Received 26 April 2022; accepted 22 September 2022; published 3 October 2022)

We analyze the effects of the long-range Coulomb interaction on the distribution of Berry curvature among the bands near charge neutrality of twisted bilayer graphene (TBG) closely aligned with hexagonal boron nitride (hBN). Due to the suppressed dispersion of the narrow bands, the band structure is strongly renormalized by electron-electron interactions, and thus, the associated topological properties of the bands are sensitive to filling. Using a Hartree formalism, we calculate the linear and nonlinear Hall conductivities, and find that for certain fillings, the remote bands contribute substantially to the Hall currents while the contribution from the central bands is suppressed. In particular, we find that these currents are generically substantial near regions of energies where the bands are highly entangled with each other, often featuring doping-induced band inversions. Our results demonstrate that topological transport in TBG/hBN is substantially modified by electron-electron interactions, which offer a simple explanation to recent experimental results.

DOI: 10.1103/PhysRevB.106.L161101

Introduction. Transverse Hall currents are usually associated with broken time-reversal symmetry. However, Hall-like currents are possible in time-reversal symmetric settings with broken inversion symmetry at second order in the applied in-plane electric field [1–4]. This so-called nonlinear Hall effect has been observed in transition-metal dichalcogenides (TMDs) [5–8] and other two-dimensional materials [9–15]. Furthermore, it has been recently shown that uniaxial strains can enhance the Berry dipole [16–18], defined as the gradient of the Berry curvature, in TMD that is responsible for the nonlinear Hall effect. For these materials, orbital valley magnetization [18,19], giant magneto-optical effects [20], and nonlinear Nernst effects [21,22] can also be induced with an applied field due to the sizable Berry dipole.

Recent theoretical studies have shown that nonlinear Hall effects can also arise in gapped and strained twisted bilayer graphene (TBG) [23–25], which depend sensitively on filling, and can be larger than in TMDs. The magnitude of the Berry dipole is predicted to be larger near half filling of the narrow conduction and valence bands. However, a recent experiment observes nonlinear Hall currents in TBG on hexagonal boron nitride (hBN) with negligible contribution from the narrow bands [26]. On the contrary, large nonlinear Hall currents are observed when the chemical potential is tuned to a spectral region entangled with the remote bands. On the basis of their experimental results, the authors of Ref. [26] suggest that the nonlinear Hall effect is due primarily to skew scattering from dynamic disorders [13] instead of a pure Berry dipole induced by a heteroaxial strain and a mass gap [27]. In addition to TBG, nonlinear Hall currents have also been measured in the related system of strained twisted double bilayer graphene (TDBG) [28]. This experiment in particular finds that the *sign* of the Berry dipole is sensitive to band inversions, and therefore is a signature of topological band transitions [29].

Inspired by these experiments, we theoretically study strained TBG in the presence of an hBN substrate. Our results indicate that the Berry dipole contributes significantly to the large nonlinear Hall effect found in the experiment of Ref. [26] and is strongly enhanced near avoided band crossings similar to the behavior of TDBG in Refs. [28,30]. Without invoking any extrinsic influence from disorder, we find that the combination of a small uniaxial heterostrain, an hBN substrate, and electron-electron interactions treated within a self-consistent Hartree formalism are enough to explain the large observed nonlinear Hall currents derived from the remote bands [26]. In particular, we find that the Coulomb interaction simultaneously distorts the energy spectrum and redistributes the Berry curvature, both of which can lead to large nonlinear Hall currents. Our paper demonstrates that because of significant interaction-meditated band distortions, the strong Coulomb repulsion in twistronic systems is not only important for inherently many-body phenomena like magnetism and superconductivity, but is also crucial for determining physics that is often otherwise studied from a single-particle perspective.

Symmetries in strained TBG/hBN. In pristine TBG graphene, both time-reversal and inversion symmetries are preserved, as shown in Fig. 1(a). For small twist angles, there are two narrow bands near charge neutrality that are connected by two Dirac points at the corners of the moiré Brillouin zone

*ppantaleon@uabc.edu.mx
†vophong@sas.upenn.edu

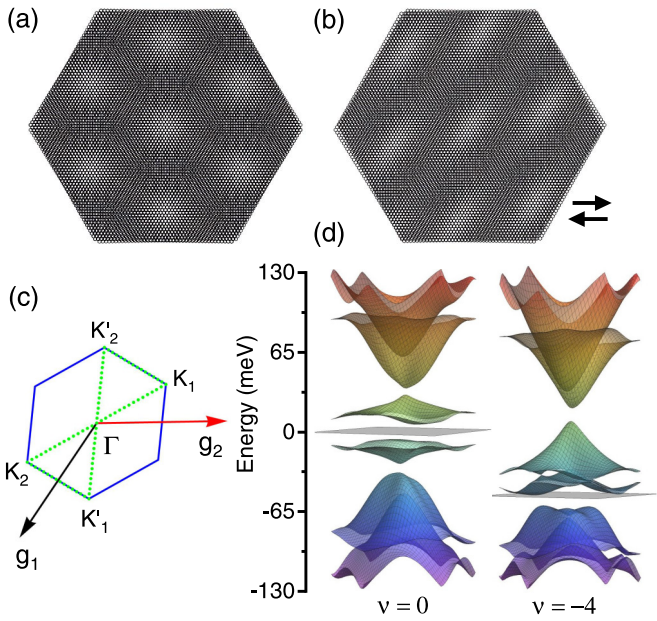

FIG. 1. (a) Schematic of the moiré superlattice for unstrained TBG and (b) heteroaxially strained TBG, where for visual clarity, we set $\epsilon = 3\%$ for the relative strain magnitude and $\phi = 0$ for the strain direction. We are assuming that the moiré pattern of the hBN substrate is the same as TBG (see Supplemental Material [31] for details). In (b), black arrows indicate the heterostrain directions. (c) Distorted moiré Brillouin zone where the reciprocal lattice vectors $\boldsymbol{g}_{1,2}$ are indicated. Green-dotted path is used to calculate the band structure. (d) Three-dimensional plots of the band structure showing six central bands for strained TBG with $\epsilon = 0.2\%$ and $\phi = 0$ suspended on hBN and for filling factors $\nu = 0$ (left) and $\nu = -4$ (right). The Fermi levels are indicated by the square shaded meshes.

(mBZ). These Dirac points are protected by a robust $\mathcal{C}_{2z}\mathcal{T}$ symmetry, where $\mathcal{C}_{2z}$ is twofold rotation about the z-axis and $\mathcal{T}$ is time reversal [32]. To gap out these Dirac points and obtain finite Berry curvature in the narrow bands, we need to break $\mathcal{C}_{2z}\mathcal{T}$ by placing TBG on hBN [33–39]. The inversion-broken character of hBN due to sublattice inequivalence is transmitted to the graphene bands by means of scalar, mass, and strain potentials [40–43]. While the magnitude of these inversion-broken gaps are extremely sensitive to the degree of alignment between TBG and hBN, they are nonzero even for a large misalignment [44]. In this paper, we use the parameters for hBN-induced potentials on TBG calculated from atomistic tight-binding modeling done in Ref. [44].

Another important feature of TBG that was experimentally determined by STM measurements is the presence of a strain field that alternates sign between the two layers (uniaxial heterostrain) and a magnitude between 0.1 and 0.5% [45–50]. Such a strain field further breaks $\mathcal{C}_{3z}$, $\mathcal{C}_{2x}$, and $\mathcal{C}_{2y}$ rotation symmetries. However, $\mathcal{C}_{2z}$ remains intact under strain, as demonstrated in Fig. 1(b). In momentum space, strain distorts the mBZ as shown in Fig. 1(c). The Dirac cones of the distorted lattice are no longer at the same energy or at the corners of the mBZ [51–53]. When both valleys are considered, TBG both with and without strain respect $\mathcal{T}$ symmetry. Therefore, only the nonlinear Hall effect can survive since the linear Hall term is odd under time reversal. In what follows, when we calculate the linear term, it will always be for a single valley, which can be nonzero since each valley individually breaks $\mathcal{T}$. In a transport experiment, both valleys are measured simultaneously; so the leading contribution to the Hall currents comes at second order in the applied electric field.

Coulomb interactions in strained TBG/hBN. In transport experiments on TBG, the Fermi level can be tuned. Due to long-range electron-electron interactions, it has been theoretically predicted [54–56] and experimentally found [45,47,57,58] that the Fermi level is "pinned" to the van Hove singularities. Away from charge neutrality, it has been shown that the Coulomb interaction is comparable or even larger than the bandwidth of the central bands, giving rise to a filling-dependent Hartree potential that substantially modifies the shape of the electronic bands [55,56]. In strained TBG/hBN with a Hartree interaction, the band structure strongly depends on the position of the Fermi level, as shown in Figs. 1(d) and 2, and in the Supplemental Material [31]. This implies that any physical quantity involving a variation of the chemical potential near or within the narrow bands in pristine TBG or TBG/hBN should account for the variation of the Hartree potential.

Linear and nonlinear Hall currents. With the preceding considerations, we now calculate the topological currents arising from the Berry curvature with electron-electron interaction encoded in a self-consistent Hartree potential. In this setting, within the semiclassical transport theory in the presence of an AC electric field $\mathcal{E}(t) = \mathrm{Re}\{\boldsymbol{\xi} e^{i\omega t}\}$ with frequency ω, the band velocity is given by $\hbar \boldsymbol{v}_n(\boldsymbol{k}) = \nabla_k E_n(\boldsymbol{k}) + e\mathcal{E} \times \boldsymbol{\Omega}_n(\boldsymbol{k})$, where the first term is the usual group velocity and the second is an anomalous term driven by a nonzero Berry curvature [59]. For us, $\boldsymbol{\xi}$ is a real vector. The band velocity $\boldsymbol{v}_n(\boldsymbol{k})$ has a component transverse to the electric field that gives rise to Hall currents. The Berry curvature for the electronic Bloch states of the nth band is $\Omega^z_{n,\mu}(\boldsymbol{k}) = 2\mathrm{Im}\langle \partial_{k_x} \Psi_{n\boldsymbol{k},\mu} | \partial_{k_y} \Psi_{n\boldsymbol{k},\mu} \rangle \hat{z}$, where we have introduced an index μ to emphasize that the Berry curvature depends on μ via the Hartree potential. Following Refs. [1,2,13,60], the transverse currents up to second order in the electric field are $\mathcal{J}_{a,\mu} = \mathrm{Re}\{\mathcal{J}^0_{a,\mu} + \mathcal{J}^{\omega}_{a,\mu} e^{i\omega t} + \mathcal{J}^{2\omega}_{a,\mu} e^{i2\omega t}\}$ with a rectified component $\mathcal{J}^0_{a,\mu} = \chi^{\mu}_{abc} \xi_b \xi^*_c$, a linear term $\mathcal{J}^{\omega}_{a,\mu} = \sigma^{\mu}_{ab} \xi_b$, and a second-harmonic component $\mathcal{J}^{2\omega}_{a,\mu} = \chi^{\mu}_{abc} \xi_b \xi_c$. The linear term contains the usual valley Hall conductivity. The susceptibility in the first and third term is given by $\chi^{\mu}_{abc} = -\frac{e^3\tau}{2\hbar^2} \epsilon^{acd} D_{bd,\mu}$ with Berry dipole (see Sec. III in the Supplemental Material [31]),

$$D_{bd,\mu} = \sum_n \int \frac{d\boldsymbol{k}}{(2\pi)^2} \Omega^d_{n,\mu}(\boldsymbol{k}) \partial_b f_0[\epsilon_{n,\mu}(\boldsymbol{k})]. \tag{1}$$

Notice that contrary to a system with rigid bands [23,24], the wavefunctions required to obtain the Berry curvature must be calculated self-consistently for each value of the Fermi energy, as shown in Fig. 2. The Berry dipole depends on the chemical potential in two different ways. The first is an explicit dependence in f_0 in the integral. The second is an *implicit* dependence due to the redistribution of the Berry curvature as charges reorganize due electrostatic interactions when electrons are added to or removed from the system (see

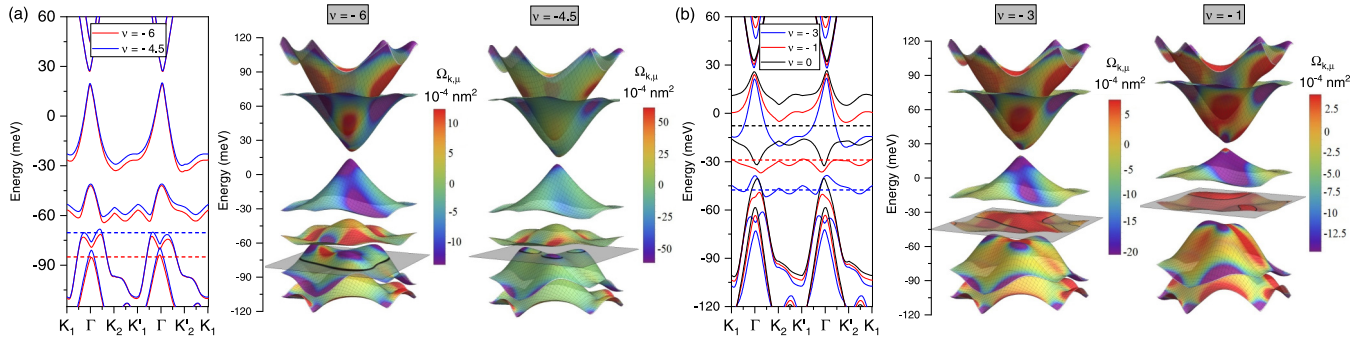

FIG. 2. Band structure of strained TBG/hBN for twist angle $\theta = 1.05^\circ$ and for different filling factors. (a) For a Fermi level within the remote bands, there are massive Dirac cones (with small masses) that significantly contribute to the Berry curvature. In (b), we show the bands for fillings within the lower narrow band. The dashed-horizontal lines in each plot are the positions of the Fermi level. Adjacent to each plot, we display the full band structure for the corresponding filling. The color texture in each band is the magnitude of the Berry curvature as indicated in the color bar. Gray-square surfaces indicate the positions of the chemical potential and black contours their intersection with the energy bands. In all plots, we use a relative strain magnitude $\epsilon = 0.2\%$ with direction $\phi = 0$.

Supplemental Material [31]). In rigid platforms where these electrostatic interactions can be neglected like in TMDs, the implicit dependence can be ignored. However, interestingly in our case, the redistribution of the Berry curvature when μ varies plays a crucial role in determining the magnitude of the nonlinear Hall effect.

Interaction-enhanced topological Hall effects. Figure 3 summarizes the topological Hall effects in strained TBG/hBN as a function of μ for an energy window covering the six central bands. Figures 3(a) and 3(e) show the valley Hall conductivity for the rigid system (TBG/hBN without interactions or strain) at $\theta = 1.05^\circ$ and $\theta = 0.95^\circ$ respectively. Figures 3(b) and 3(f) show the corresponding Hall conductivity with interactions; there, the behavior is especially different compared to the rigid system near $\nu = \pm 4$. For instance, the Hall conductivity at $\nu = -4$ and $\theta = 0.95^\circ$ vanishes when interactions are neglected, but is about $-2e^2/h$ when interactions are included. In addition, the range of chemical potential that resides in the central bands is significantly widened by the Hartree potential [54]. We also note that whenever the chemical potential is inside a bulk mobility gap, σ^{μ}_{xy} is quantized and is given by the Chern numbers of the bands below chemical potential. The Chern numbers of the six bands closest to charge neutrality are tabulated in Figs. 3(h) and 3(i).

Further straining the system in addition to the Hartree potential does not significantly change σ^{μ}_{xy}, as shown by the black lines in Figs. 3(b) and 3(f). Therefore, strain seems to play a minimal role in the linear valley Hall effect. On the contrary,

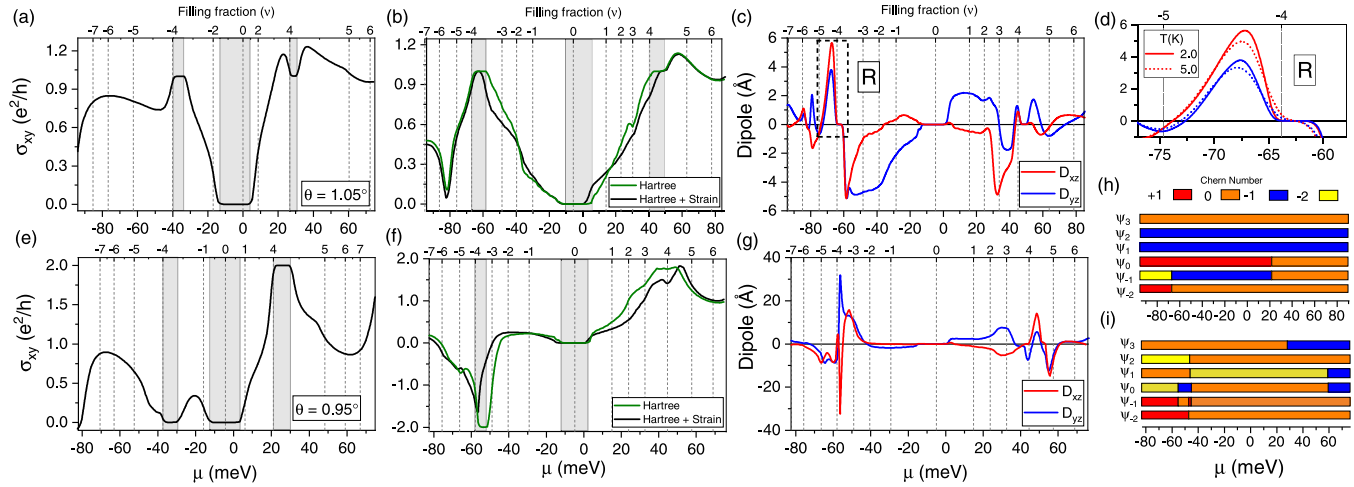

FIG. 3. Interaction-enhanced topological Hall effects in TBG/hBN. In the top row, for a twist angle of $\theta = 1.05^\circ$, we plot the valley Hall conductivity as a function of chemical potential for (a) the rigid system and (b) with interactions and strain. Gray-shaded areas are gapped regions without strain. In (c), we display the Berry dipole as a function of μ. In (d), we show an enlarged region of (c), labeled as R, where the dependence on temperature is indicated. Bottom row is for a twist angle $\theta = 0.95^\circ$, where we plot the valley Hall conductivity for (e) the rigid system and (f) with interactions and strain. (g) Berry dipole featuring a prominent peak near $\nu = -4$. Panels (h) and (i) display the Chern numbers of the six central bands, with ψ_i, where $i = -2, ..., 3$, labeling the bands from lower to higher energy, as a function of μ for (h) $\theta = 1.05^\circ$ and (i) $\theta = 0.95^\circ$. Several doping-induced band inversions are observed. In all plots, unless otherwise indicated, we use $T = 5$ K, $\epsilon_d = 10$ for the dielectric constant, and $\epsilon = 0.2\%$ and $\phi = 0$ for strain. All calculations are done for one spin species in a single valley. For a comparison with the noninteracting case, please see Figs. S5 and S6 in the Supplemental Material [31].

strain is crucial for the nonlinear Hall effect since it permits a nonzero Berry dipole to develop, as shown in Figs. 3(c) and 3(g). In contrast to earlier noninteracting calculations [23,24] where the Berry dipole near magic angle is found to be large especially when the Fermi level is within the narrow bands (see also Fig. S6 within the Supplemental Material [31]), we find in the present study using realistic parameters that the Hartree potential enhances the Berry dipole near the edges of the narrow central bands. The Berry dipole is large when either the Berry curvature, the band velocity, or both are large near the Fermi surface. Furthermore, the Berry curvature can also be made large when the energy separation between occupied and unoccupied bands is very small. Therefore, the Berry dipole peaks where either (i) the group velocity is large or (ii) the energy bands are very close together. The former contribution generically occurs where an initial band crossing (such as a Dirac cone) is gapped out by some symmetry-breaking perturbations, which is the case for $\nu = -4.5$ as shown in Fig. 2(a). The latter contribution comes from regions in energies where the bands are highly entangled so that the separation between occupied and unoccupied bands is quite small. This is the case for $\nu = -6$ in Fig. 2(a). These two contributions are generically large near band edges, which intuitively explains why we often observe large nonlinear Hall responses for ν near -4.

In Figs. 3(c) and 3(g), the Berry dipole pseudovector $\boldsymbol{D}_\mu = (D_{xz,\mu}, D_{yz,\mu})$ is defined relative to the lattice structure. In an experiment, it is difficult to isolate the effect of either component of the Berry dipole. Instead, an applied electric field $\boldsymbol{\xi}$ at a generic angle γ relative to the crystallographic axes mixes these components such that the effective angle-dependent susceptibility is $\chi^{\mu}_{\text{eff}}(\gamma) = -4\frac{e^3\tau}{2\hbar^2}\boldsymbol{D}_\mu \cdot \hat{\boldsymbol{\xi}}$, where the prefactor 4 accounts for spin and valley degeneracies. The effective susceptibility for various field angles γ at different twist angles θ are plotted in Fig. 4. We emphasize a few interesting features. First, χ^{μ}_{eff} is concentrated in highly-entangled spectral regions, especially for small angles. This enhancement is sometimes made possible by *doping-induced* band inversions, For instance, near $\mu = -67$ meV, we see in Fig. 3(h) that there is a band inversion between bands ψ_{-2} and ψ_{-1}, resulting in a large susceptibility shown in Fig. 4(b). Second, a change in the *sign* of χ^{μ}_{eff} indicates a change in the local (but not necessarily global) band geometry near the Fermi surface. For example, we see that χ^{μ}_{eff} changes sign near $\nu = -4$ at $\theta = 1.05°$. This is precisely the energy region where the linear Hall conductivity [shown in Fig. 3(b)] reaches a maximum, signifying a change in the sign of the Berry curvature. This reversal in local band geometry can occur both as μ sweeps across a bulk gap, such as the case near $\nu = -4$ at $\theta = 1.05°$, and as μ varies within a single bulk band, such as the case near $\nu = -1.8$ at $\theta = 1.05°$ and $\gamma = 0$ or π [61]. Similar polarity reversals are observed for $\theta = 0.95°$ and $\theta = 1.12°$ as well. The effects for different strain values are shown in the Supplemental Material [31].

Discussion and conclusions. Our results are in qualitative agreement [62] with the recent experiment in TBG [26] where a large nonlinear Hall current is observed when the chemical potential is tuned to a spectral region entangled with the remote bands. The authors of the experiment attribute this observation to skew scattering due to magnetic impurities. However, we can explain the large observed signals at the edges of the narrow bands by carefully accounting for band structure renormalization due to the Hartree potential and the presence of an hBN substrate without considering disorder. Our theory cannot exclude the role of disorder in the experimental results, but it at least demonstrates that the Berry dipole also contributes significantly to the Hall current at filling factors near ± 4 if hBN is nearly aligned with TBG. Importantly, the source of this Berry dipole enhancement is unquestionably Coulomb repulsion. In addition, our result is also of general agreement to the conclusions of Refs. [28,30] that the Berry dipole is sensitive to band inversions, although our topological transitions are induced by doping instead of a bias. Nonetheless, this result demonstrates that although the Berry dipole is a Fermi surface property, it can sometimes be used to infer global band topology. Furthermore, the inclusion of the Fock term, which is known to give rise to various symmetry-broken ground states, warrants further investigation in future works. However, it is not expected that the Fock term will play a dominant role for fillings far away from charge neutrality on the basis of earlier calculations [63]. Therefore, we believe the calculations presented in this paper already capture the salient features of the nonlinear Hall effect in TBG. Encouraged by this, we believe that adopting the theoretical framework developed here to study nonlinear Hall effects, and other effects, which depend on the distribution of the local Berry curvature such as the orbital magnetization [64], in other experimentally-relevant twisted

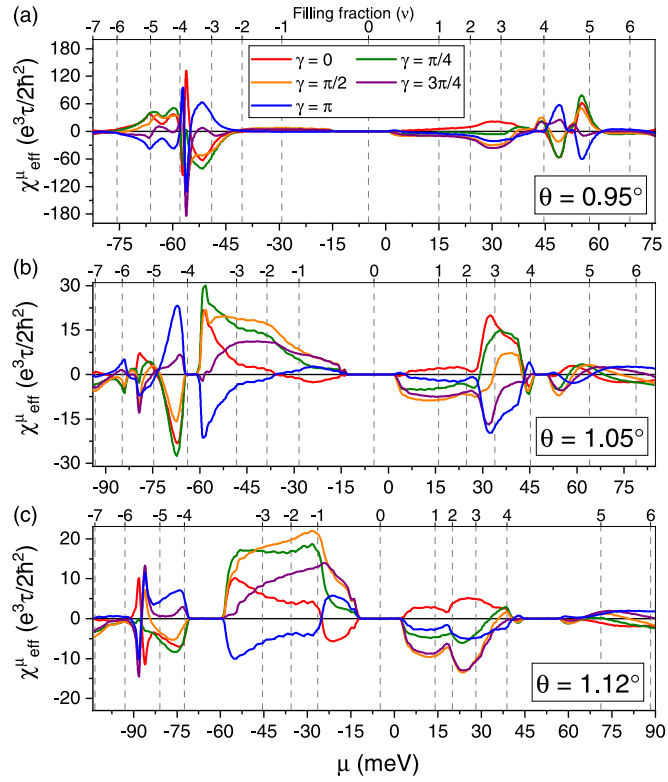

FIG. 4. Effective nonlinear susceptibility in strained TBG/hBN for different current directions with (a) $\theta = 0.95°$, (b) $\theta = 1.05°$, and (c) $\theta = 1.12°$. For small twist angles, the Berry dipole is strongly enhanced near $\nu = \pm 4$.

two-dimensional materials is a promising future research direction.

Acknowledgments. IMDEA Nanociencia acknowledges support from the "Severo Ochoa" Programme for Centres of Excellence in R&D (Grant No. SEV-2016-0686). P.A.P and F.G. acknowledge funding from the European Commission, within the Graphene Flagship, Core 3, Grant No. 881603 and from Grants NMAT2D (Comunidad de Madrid, Spain), SprQuMat. V.T.P. acknowledges support from the NSF Graduate Research Fellowships Program and the P.D. Soros Fellowship for New Americans. G.N. thanks UNAM-DGAPA Project No. IN102620 and CONACyT Project No. 1564464.

[1] T. Low, Y. Jiang, and F. Guinea, Topological currents in black phosphorus with broken inversion symmetry, Phys. Rev. B **92**, 235447 (2015).

[2] I. Sodemann and L. Fu, Quantum Nonlinear Hall Effect Induced by Berry Curvature Dipole in Time-Reversal Invariant Materials, Phys. Rev. Lett. **115**, 216806 (2015).

[3] S. Nandy and I. Sodemann, Symmetry and quantum kinetics of the nonlinear Hall effect, Phys. Rev. B **100**, 195117 (2019).

[4] Z. Z. Du, H.-Z. Lu, and X. C. Xie, Nonlinear Hall effects, Nat. Rev. Phys. **3**, 744 (2021).

[5] Q. Ma, S. Y. Xu, H. Shen, D. MacNeill, V. Fatemi, T. R. Chang, A. M. Mier Valdivia, S. Wu, Z. Du, C. H. Hsu *et al.*, Observation of the nonlinear Hall effect under time-reversal-symmetric conditions, Nature (London) **565**, 337 (2019).

[6] K. Kang, T. Li, E. Sohn, J. Shan, and K. F. Mak, Nonlinear anomalous Hall effect in few-layer WTe_2, Nat. Mater. **18**, 324 (2019).

[7] M. Huang, Z. Wu, J. Hu, X. Cai, E. Li, L. An, X. Feng, Z. Ye, N. Lin, K. T. Law, and N. Wang, Giant nonlinear Hall effect in twisted WSe_2, arXiv:2006.05615.

[8] J.-X. Hu, C.-P. Zhang, Y.-M. Xie, and K. T. Law, Nonlinear Hall effects in strained twisted bilayer WSe_2, arXiv:2004.14140.

[9] Y. Araki, Strain-induced nonlinear spin Hall effect in topological Dirac semimetal, Sci. Rep. **8**, 15236 (2018).

[10] R.-C. Xiao, D.-F. Shao, Z.-Q. Zhang, and H. Jiang, Two-Dimensional Metals for Piezoelectriclike Devices Based on Berry-Curvature Dipole, Phys. Rev. Appl. **13**, 044014 (2020).

[11] J. I. Facio, D. Efremov, K. Koepernik, J.-S. You, I. Sodemann, and J. van den Brink, Strongly Enhanced Berry Dipole at Topological Phase Transitions in BiTeI, Phys. Rev. Lett. **121**, 246403 (2018).

[12] H. Wang and X. Qian, Ferroelectric nonlinear anomalous Hall effect in few-layer WTe_2, npj Comput. Mater. **5**, 1 (2019).

[13] Z. Z. Du, C. M. Wang, S. Li, H. Z. Lu, and X. C. Xie, Disorder-induced nonlinear Hall effect with time-reversal symmetry, Nat. Commun. **10**, 3047 (2019).

[14] Z.-S. Liao, H.-H. Zhang, and Z. Yan, Nonlinear Hall effect in two-dimensional class-AI metals, Phys. Rev. B **103**, 235151 (2021).

[15] N. B. Joseph, S. Roy, and A. Narayan, Tunable topology and Berry curvature dipole in transition metal dichalcogenide janus monolayers, Mater. Res. Express **8**, 124001 (2021).

[16] J.-S. You, S. Fang, S.-Y. Xu, E. Kaxiras, and T. Low, Berry curvature dipole current in the transition metal dichalcogenides family, Phys. Rev. B **98**, 121109(R) (2018).

[17] B. T. Zhou, C.-P. Zhang, and K. T. Law, Highly tunable nonlinear Hall effects induced by spin-orbit couplings in strained polar transition-metal dichalcogenides, Phys. Rev. Appl. **13**, 024053 (2020).

[18] J. Son, K.-H. Kim, Y. H. Ahn, H.-W. Lee, and J. Lee, Strain Engineering of the Berry Curvature Dipole and Valley Magnetization in Monolayer MoS_2, Phys. Rev. Lett. **123**, 036806 (2019).

[19] L.-k. Shi and J. C. W. Song, Symmetry, spin-texture, and tunable quantum geometry in a Wte_2 monolayer, Phys. Rev. B **99**, 035403 (2019).

[20] J. Liu and X. Dai, Anomalous Hall effect, magneto-optical properties, and nonlinear optical properties of twisted graphene systems, npj Comput. Mater. **6**, 57 (2020).

[21] X.-Q. Yu, Z.-G. Zhu, J.-S. You, T. Low, and G. Su, Topological nonlinear anomalous nernst effect in strained transition metal dichalcogenides, Phys. Rev. B **99**, 201410(R) (2019).

[22] C. Zeng, S. Nandy, A. Taraphder, and S. Tewari, Nonlinear Nernst effect in bilayer WTe_2, Phys. Rev. B **100**, 245102 (2019).

[23] P. A. Pantaleón, T. Low, and F. Guinea, Tunable large Berry dipole in strained twisted bilayer graphene, Phys. Rev. B **103**, 205403 (2021).

[24] C.-P. Zhang, J. Xiao, B. T. Zhou, J.-X. Hu, Y.-M. Xie, B. Yan, and K. T. Law, Giant nonlinear Hall effect in strained twisted bilayer graphene, arXiv:2010.08333.

[25] A. Arora, J. F. Kong, and J. C. W. Song, Strain-induced large injection current in twisted bilayer graphene, Phys. Rev. B **104**, L241404 (2021).

[26] J. Duan, Y. Jian, Y. Gao, H. Peng, J. Zhong, Q. Feng, and Y. Yao, Giant second-order nonlinearity of chiral Bloch electrons in twisted bilayer graphene, arXiv:2201.09274.

[27] In fact, the authors of Ref. [26] do not consider strain. So their system retains some twofold rotations that force the Berry dipole to vanish. They justify this exclusion by arguing that the contribution from strain is much smaller than the extrinsic contributions.

[28] S. Sinha, P. C. Adak, A. Chakraborty, K. Das, K. Debnath, L. D. V. Sangani, K. Watanabe, T. Taniguchi, U. V. Waghmare, A. Agarwal, and M. M. Deshmukh, Berry curvature dipole senses topological transition in a moiré superlattice, Nat. Phys. **18**, 765 (2022).

[29] In TDBG, these band inversions can be induced by applying an interlayer bias voltage. When the bias is large enough, the active middle bands can hybridize with the remote bands and create a sign change in the local Berry curvature.

[30] A. Chakraborty, K. Das, S. Sinha, P. C. Adak, M. M. Deshmukh, and A. Agarwal, Nonlinear anomalous Hall effects probe topological phase-transitions in twisted double bilayer graphene, arXiv:2205.15120.

[31] See Supplemental Material at http://link.aps.org/supplemental/10.1103/PhysRevB.106.L161101 for discussion of the Hartree formalism that includes strain and hBN alignment, numerical estimates of the relevant parameters, and additional results for

both the noninteracting and interacting systems, which cites Refs. [1,2,13,23,24,26,28,33,40,41,44,51,52,54,55,60,65–75].

[32] We note that although both $\mathcal{C}_{2z}$ and $\mathcal{T}$ map one valley to the other, the combination $\mathcal{C}_{2z}\mathcal{T}$ preserves the valley index.

[33] T. Cea, P. A. Pantaleón, and F. Guinea, Band structure of twisted bilayer graphene on hexagonal boron nitride, Phys. Rev. B **102**, 155136 (2020).

[34] Y.-H. Zhang, D. Mao, and T. Senthil, Twisted Bilayer Graphene Aligned with Hexagonal Boron Nitride: Anomalous Hall Effect and a Lattice Model, Phys. Rev. Res. **1**, 033126 (2019).

[35] J. Shi, J. Zhu, and A. H. MacDonald, Moiré commensurability and the quantum anomalous Hall effect in twisted bilayer graphene on hexagonal boron nitride, Phys. Rev. B **103**, 075122 (2021).

[36] A. L. Sharpe, E. J. Fox, A. W. Barnard, J. Finney, K. Watanabe, T. Taniguchi, M. A. Kastner, and D. Goldhaber-Gordon, Evidence of orbital ferromagnetism in twisted bilayer graphene aligned to hexagonal boron nitride, Nano Lett. **21**, 4299 (2021).

[37] X. Huang, L. Chen, S. Tang, C. Jiang, C. Chen, H. Wang, Z.-X. Shen, H. Wang, and Y.-T. Cui, Imaging dual-moiré lattices in twisted bilayer graphene aligned on hexagonal boron nitride using microwave impedance microscopy, Nano Lett. **21**, 4292 (2021).

[38] X. Lin and J. Ni, Symmetry breaking in the double moiré superlattices of relaxed twisted bilayer graphene on hexagonal boron nitride, Phys. Rev. B **102**, 035441 (2020).

[39] X. Lin, K. Su, and J. Ni, Misalignment instability in magic-angle twisted bilayer graphene on hexagonal boron nitride, 2D Mater. **8**, 025025 (2021).

[40] J. R. Wallbank, A. A. Patel, M. Mucha-Kruczyński, A. K. Geim, and V. I. Fal'Ko, Generic miniband structure of graphene on a hexagonal substrate, Phys. Rev. B **87**, 245408 (2013).

[41] P. San-Jose, A. Gutiérrez-Rubio, M. Sturla, and F. Guinea, Spontaneous strains and gap in graphene on boron nitride, Phys. Rev. B **90**, 075428 (2014).

[42] M. Mucha-Kruczyński, J. R. Wallbank, and V. I. Fal'Ko, Heterostructures of bilayer graphene and h-BN: Interplay between misalignment, interlayer asymmetry, and trigonal warping, Phys. Rev. B **88**, 205418 (2013).

[43] J. Jung, E. Laksono, A. M. Dasilva, A. H. Macdonald, M. Mucha-Kruczyński, and S. Adam, Moiré band model and band gaps of graphene on hexagonal boron nitride, Phys. Rev. B **96**, 085442 (2017).

[44] M. Long, P. A. Pantaleón, Z. Zhan, F. Guinea, J. Á. Silva-Guillén, and S. Yuan, An atomistic approach for the structural and electronic properties of twisted bilayer graphene-boron nitride heterostructures, npj Comput. Mater. **8**, 73 (2022).

[45] Y. Jiang, X. Lai, K. Watanabe, T. Taniguchi, K. Haule, J. Mao, and E. Y. Andrei, Charge order and broken rotational symmetry in magic-angle twisted bilayer graphene, Nature (London) **573**, 91 (2019).

[46] Y. Choi, J. Kemmer, Y. Peng, A. Thomson, H. Arora, R. Polski, Y. Zhang, H. Ren, J. Alicea, G. Refael *et al.*, Electronic correlations in twisted bilayer graphene near the magic angle, Nat. Phys. **15**, 1174 (2019).

[47] Y. Xie, B. Lian, B. Jäck, X. Liu, C. L. Chiu, K. Watanabe, T. Taniguchi, B. A. Bernevig, and A. Yazdani, Spectroscopic signatures of many-body correlations in magic-angle twisted bilayer graphene, Nature (London) **572**, 101 (2019).

[48] A. Kerelsky, L. J. McGilly, D. M. Kennes, L. Xian, M. Yankowitz, S. Chen, K. Watanabe, T. Taniguchi, J. Hone, C. Dean *et al.*, Maximized electron interactions at the magic angle in twisted bilayer graphene, Nature (London) **572**, 95 (2019).

[49] J.-B. Qiao, L.-J. Yin, and L. He, Twisted graphene bilayer around the first magic angle engineered by heterostrain, Phys. Rev. B **98**, 235402 (2018).

[50] L. Huder, A. Artaud, T. Le Quang, G. T. de Laissardière, A. G. M. Jansen, G. Lapertot, C. Chapelier, and V. T. Renard, Electronic Spectrum of Twisted Graphene Layers under Heterostrain, Phys. Rev. Lett. **120**, 156405 (2018).

[51] M. Oliva-Leyva and G. G. Naumis, Generalizing the Fermi velocity of strained graphene from uniform to nonuniform strain, Phys. Lett. A **379**, 2645 (2015).

[52] Z. Bi, N. F. Q. Yuan, and L. Fu, Designing flat bands by strain, Phys. Rev. B **100**, 035448 (2019).

[53] D. E. Parker, T. Soejima, J. Hauschild, M. P. Zaletel, and N. Bultinck, Strain-Induced Quantum Phase Transitions in Magic-Angle Graphene, Phys. Rev. Lett. **127**, 027601 (2021).

[54] T. Cea, N. R. Walet, and F. Guinea, Electronic band structure and pinning of Fermi energy to Van Hove singularities in twisted bilayer graphene: A self-consistent approach, Phys. Rev. B **100**, 205113 (2019).

[55] F. Guinea and N. R. Walet, Electrostatic effects, band distortions, and superconductivity in twisted graphene bilayers, Proc. Natl. Acad. Sci. USA **115**, 13174 (2018).

[56] L. Rademaker, D. A. Abanin, and P. Mellado, Charge smoothening and band flattening due to Hartree corrections in twisted bilayer graphene, Phys. Rev. B **100**, 205114 (2019).

[57] S. L. Tomarken, Y. Cao, A. Demir, K. Watanabe, T. Taniguchi, P. Jarillo-Herrero, and R. C. Ashoori, Electronic Compressibility of Magic-Angle Graphene Superlattices, Phys. Rev. Lett. **123**, 046601 (2019).

[58] X. Lu, P. Stepanov, W. Yang, M. Xie, M. A. Aamir, I. Das, C. Urgell, K. Watanabe, T. Taniguchi, G. Zhang, A. Bachtold *et al.*, Superconductors, orbital magnets and correlated states in magic-angle bilayer graphene, Nature (London) **574**, 653 (2019).

[59] D. Xiao, M.-C. Chang, and Q. Niu, Berry phase effects on electronic properties, Rev. Mod. Phys. **82**, 1959 (2010).

[60] Z. Z. Du, C. M. Wang, H.-P. Sun, H.-Z. Lu, and X. C. Xie, Quantum theory of the nonlinear Hall effect, Nat. Commun. **12**, 5038 (2021).

[61] When there is an external tunable parameter such as an interlayer bias voltage, the sign of the Berry dipole can also be used to detect the occurrence of a band inversion driven by that parameter. This is precisely the case in Ref. [28].

[62] Quantitatively reproducing the experimental measurements from our theory is more challenging because the scattering time is not empirically known and is difficult to calculate from first principles. In addition, there are several adjustable parameters in the setup that can complicate a quantitative comparison such as the degree of alignment between TBG and the substrate and the direction and magnitude of strain relative to the lattice. Nonetheless, we have made some rough numerical estimates in Ref. [31] that suggest a sensible order-of-magnitude agreement.

[63] T. Cea and F. Guinea, Band structure and insulating states driven by Coulomb interaction in twisted bilayer graphene, Phys. Rev. B **102**, 045107 (2020).

[64] S. Grover, M. Bocarsly, A. Uri, P. Stepanov, G. Di Battista, I. Roy, J. Xiao, A. Y. Meltzer, Y. Myasoedov, K. Pareek *et al.*, Chern mosaic and Berry-curvature magnetism in magic-angle graphene, Nat. Phys. **18**, 885 (2022).

[65] M. Mannaï and S. Haddad, Twistronics versus straintronics in twisted bilayers of graphene and transition metal dichalcogenides, Phys. Rev. B **103**, L201112 (2021).

[66] R. Faccio, P. A. Denis, H. Pardo, C. Goyenola, and Á. W. Mombrú, Mechanical properties of graphene nanoribbons, J. Phys.: Condens. Matter **21**, 285304 (2009).

[67] M. Oliva-Leyva and G. G. Naumis, Understanding electron behavior in strained graphene as a reciprocal space distortion, Phys. Rev. B **88**, 085430 (2013).

[68] G. G. Naumis, S. Barraza-Lopez, M. Oliva-Leyva, and H. Terrones, Electronic and optical properties of strained graphene and other strained 2D materials: A review, Rep. Prog. Phys. **80**, 096501 (2017).

[69] F. Guinea, F. Katsnelson, and A. Geim, Energy gaps and a zero-field quantum Hall effect in graphene by strain engineering, Nat. Phys. **6**, 30 (2010).

[70] N. N. T. Nam and M. Koshino, Lattice relaxation and energy band modulation in twisted bilayer graphene, Phys. Rev. B **96**, 075311 (2017).

[71] M. Koshino, N. F. Yuan, T. Koretsune, M. Ochi, K. Kuroki, and L. Fu, Maximally Localized Wannier Orbitals and the Extended Hubbard Model for Twisted Bilayer Graphene, Phys. Rev. X **8**, 031087 (2018).

[72] G. Tarnopolsky, A. J. Kruchkov, and A. Vishwanath, Origin of Magic Angles in Twisted Bilayer Graphene, Phys. Rev. Lett. **122**, 106405 (2019).

[73] D. Brida, A. Tomadin, C. Manzoni, Y. J. Kim, A. Lombardo, S. Milana, R. R. Nair, K. S. Novoselov, A. C. Ferrari, G. Cerullo, and M. Polini, Ultrafast collinear scattering and carrier multiplication in graphene, Nat. Commun. **4**, 1987 (2013).

[74] Y. Cao, V. Fatemi, S. Fang, K. Watanabe, T. Taniguchi, E. Kaxiras, and P. Jarillo-Herrero, Unconventional superconductivity in magic-angle graphene superlattices, Nature (London) **556**, 43 (2018).

[75] T. Fukui, Y. Hatsugai, and H. Suzuki, Chern numbers in discretized Brillouin zone: Efficient method of computing (spin) Hall conductances, J. Phys. Soc. Jpn. **74**, 1674 (2005).